HHS Public Access

Author manuscript

Science. Author manuscript; available in PMC 2022 November 03.

Published in final edited form as:

Science. 2022 February 04; 375(6580): 570–574. doi:10.1126/science.abm1891.

Probing subthreshold dynamics of hippocampal neurons by pulsed optogenetics

Manuel Valero[1,*], **Ipshita Zutshi**[1], **Euisik Yoon**[2,3], **György Buzsáki**[1,4,5,*]

[1]Neuroscience Institute, Langone Medical Center, New York University, New York, NY 10016, USA

[2]Department of Electrical Engineering and Computer Science, University of Michigan, Ann Arbor, MI 48109, USA

[3]Center for Nanomedicine, Institute for Basic Science (IBS) and Graduate Program of Nano Biomedical Engineering (Nano BME), Yonsei University, Seoul 03722, South Korea

[4]Neuroscience Institute and Department of Neurology, Langone Medical Center, New York, NY 10016, USA

[5]Center for Neural Science, New York University, New York, NY 10003, USA

Abstract

Understanding how excitatory (E) and inhibitory (I) inputs are integrated by neurons requires monitoring their subthreshold behavior. We probed the subthreshold dynamics using optogenetic depolarizing pulses in hippocampal neuronal assemblies in freely moving mice. Excitability decreased during sharp-wave ripples coupled with increased I. In contrast to this “negative gain,” optogenetic probing showed increased within-field excitability in place cells by weakening I and unmasked stable place fields in initially non–place cells. Neuronal assemblies active during sharp-wave ripples in the home cage predicted spatial overlap and sequences of place fields of both place cells and unmasked preexisting place fields of non–place cells during track running. Thus, indirect probing of subthreshold dynamics in neuronal populations permits the disclosing of preexisting assemblies and modes of neuronal operations.

Understanding how neurons integrate excitatory (E) and inhibitory (I) inputs requires access to the neuron’s subthreshold dynamics (1–4). Because intracellular monitoring of

[*]Corresponding author. valegarman@gmail.com (M.V.); gyorgy.buzsaki@nyumc.org (G.B.).

Author contributions: M.V. and G.B. designed the experiments. M.V. performed and analyzed the experiments with I.Z. G.B. and M.V. wrote the paper with contributions from other authors.

Competing interests: E.Y. is a cofounder of NeuroLight Technologies, a for-profit manufacturer of neurotechnology. The other authors declare no competing interests.

SUPPLEMENTARY MATERIALS

science.org/doi/10.1126/science.abm1891

Material and Methods

Figs. S1 to S15

References (40–54)

MDAR Reproducibility Checklist

View/request a protocol for this paper from Bio-protocol.

cell assemblies in behaving animals is currently unrealistic, different single-cell modes of operations (or “models”) have been proposed to explain firing characteristics in various circumstances (Fig. 1, A and B, and fig. S1) (1). In the “tuned excitation” (“blanket” inhibition) (1, 5) and “balanced network” models (I activity tracks E changes) (6–8), both membrane polarization (V_m) and firing rate response decrease at more depolarized V_m (Fig. 1, A and B) (9–11). By contrast, in the “reciprocal network” model, reduction of I is coupled to V_m depolarization and increased firing rate (Fig. 1, A and B) (12–14). Thus, by varying V_m experimentally and observing the changes in firing rates, one can gain access to the subthreshold behavior of neurons (fig. S1). Adding active conductances to the model neuron affected its quantitative features but did not change these predictions qualitatively (figs. S2 and S3).

We probed V_m with short optogenetic pulses. Using micro–light-emitting diode (μLED) probes (four shanks with three μLEDs on each shank) (15), we recorded and probed large numbers of CA1 pyramidal neurons simultaneously in freely moving calcium/calmodulin–dependent protein kinase II alpha (CamKIIα) -Cre::Ai32 mice (Fig. 1, C and D, and fig. S4; n = 822 pyramidal neurons in four mice; 43.3 ± 8.37 pyramidal neurons per session). μLEDs were activated (0.02 to 0.1 μW, 20 ms duration) with randomly variable (20 to 40 ms) offsets so that stimulation of each site reccurred at ~0.3- to 0.6-s intervals Fig. 1C and fig. S5). Random intervals (20 ms) between the light pulses served as control epochs for comparison (materials and methods). Of 822 neurons, 611 responded unequally to the three neighboring μLEDs, owing to their different distances from the recorded neurons (Fig. 1, D and E, and figs. S4 and S5), and these responses were used as a proxy for estimating relative changes of V_m and E/I dynamics. The evoked spike responses varied as a function of brains state (fig. S6) but did not perturb the firing features of the neurons (fig. S7). No changes were observed in nonresponsive neurons, safeguarding against local network-induced effects (fig. S8).

During sharp-wave ripples (SPW-Rs), excitatory neurons increased their firing rates more than inhibitory neurons (fig. S9) (6). In contrast to this population gain of excitation, light-induced spike responses in individual pyramidal cells decreased during SPW-Rs (ΔRate; Fig. 1, F to I). Increasing V_m depolarization decreased the light-induced response during SPW-Rs (Fig. 1J), resembling the balanced mode of operation (Fig. 1A). This conclusion was further supported by the negative correlation between firing-rate change during SPW-R and baseline firing rates of neurons ($\rho = -0.19$, $P < 10^{-7}$; fig. S10) and more directly by intracellular experiments, in which V_m was systematically varied (Fig. 1, K to M), reproducing the effect seen with optogenetic V_m depolarization (Fig. 1I) and favoring the balanced E/I model.

Next, we examined the subthreshold E/I dynamics of place cells. During track running, three blocks of 10 baseline runs on a linear track were interleaved with two blocks of 40 to 50 stimulation runs (fig. S7D). We observed a gain at the trough of the theta cycle, the phase corresponding to the strongest synchrony of pyramidal neurons (Fig. 2A) (16). We then compared neuronal excitability within and outside the place fields of place cells (17). With a standard definition of “place field” (materials and methods) (18), more than half of the pyramidal neurons were classified as place cells [73% and 71% of light-responsive and nonresponsive neurons, respectively; $P = 0.90$, χ^2 test; (17–19); fig. S11]. The induced

spike responses varied within and outside the place field (Fig. 2, C and D). The induced rate increase was higher within than outside the place field (Fig. 2E and fig. S12). Increasing depolarization of V_m by stronger light intensity increased the in-field gain several-fold (Fig. 2F). This in-field gain was positively correlated with both the out-of-field firing rate and the home-cage firing rate of the neuron ($\rho = 0.17$, $P < 10^{-5}$ and $\rho = 0.25$, $P < 10^{-7}$, respectively; fig S12). No rate changes were observed in nonresponsive pyramidal neurons (fig. S8). These results support the reciprocal mode of operation.

Light responses in place cells, tested in the home cage before the track, were significantly stronger than in non–place cells, and these results cannot be explained by differences in firing rate (Fig. 3A and fig. S13), suggesting that neurons with higher excitability more likely express place fields. In support of this hypothesis, optogenetic depolarization revealed place fields in the majority of non–place cells (Fig. 3, B and C; 69.3%, 289 of 417; materials and methods), although the in-field gain was less for the induced place fields than for real place fields (Fig. 3D and fig. S13). We found a robust correlation between the spatial location of induced place field spikes and the sparse spikes of non–place cells in the absence of stimulation (Fig. 3, C and E; “ghost fields”).

Features of the optogenetically unmasked place fields were similar to those of real place fields (Fig. 3, F and G, and fig. S12). To anchor neuronal firing to behavior, we examined the precision by which the animal’s position on the track can be predicted by active neurons (19). The root mean squared error of the decoded position was highest for the sparse non–place cell spikes and lowest for light-boosted spikes of place cells. The induced spikes of non–place cells more accurately predicted the mouse’s position on the track than those of “bona fide” place cells (Fig. 3H and fig. S11).

We found a reliable correlation between spatial correlations of place cell pairs on the track and firing rate correlations of the same pairs during SPW-Rs in the home cage (Fig. 4, A to C). (20). No such relationship was present for non–place cell pairs (Fig. 4C). However, during optogenetic stimulation, the relationship between cofiring during SPW-Rs and spatial overlap was revealed for unmasked place fields of non–place field pairs (Fig. 4C). To study the population consequence of the pairwise effects, we performed independent component analysis (ICA) on the Z-scored spike matrix of pyramidal neurons (21) to extract patterns of higher-order cofiring in the home cage (Fig. 4D). Assembly members of place cells, but not of mixtures of place and non–place cells, showed higher spatial correlation than chance (Fig. 4E). However, when spikes of unmasked place fields were considered, they expressed spatial correlation at the level of real place cells (Fig. 4F and fig. S14). Sequential firing of place cells was correlated with spike sequences during SPW-Rs (Fig. 4G) (22, 23). The fraction of SPW-R events with significant virtual track trajectories increased when unmasked place fields were also included for the construction of the place field sequence template (Fig. 4H).

Optogenetic depolarization of neurons increased the within-field firing rate gain in hippocampal place cells and unmasked place fields in non–place cells (1,24–26), implying that almost any pyramidal cell can express a place field and that the entire CA1 population contributes to forming specific attractors or trajectories in any given situation (1, 24, 26, 27). In these preconfigured attractors (23, 28, 29), neurons with the highest excitability form a

scaffold map and emit high-enough spike rates to be classified as place cells (17). Place cells are not continuously “driven” by outside cues (30, 31) but emerge by transient disinhibition, perhaps coupled with excitation, as predicted by the reciprocal mode of operation and further supported by the position-dependent firing rates of inhibitory interneurons as well as the decreased inhibition of place cells within their fields (fig. S15). Our results challenge the current notion of spatially uniform inhibition underlying place cell properties and reconcile several models of place field emergence (1, 25, 26, 29, 32).

Optogenetic perturbation during the theta cycles and SPW-Rs revealed opposite excitability rules, and the SPW-R data were best fitted by a balanced network model (33–35). Even though SPW-R represents the highest excitability state of the CA1 network, the contributing individual neurons decrease their excitability. This negative gain enables larger rate changes of slow firing, compared to fast firing, neurons during SPW-R. By contrast, the reciprocal mode of operation during exploration allows for larger in-field gain for faster-firing, compared to slow-firing, neurons. Brain state–dependent shifts between the reciprocal and balanced E/I modes of operations may be brought about by the altered temporal relationship between interneuron and pyramidal cell spiking and the consequent V_m (36), perhaps set by subcortical neuromodulators. SPW-R is a natural V_m changer (37) during which more neurons fire than can be accounted for by place cells active during waking experience (37–39). These spikes are emitted by those neurons whose sparse spiking activity also contributes to the same hippocampal map.

Supplementary Material

Refer to Web version on PubMed Central for supplementary material.

ACKNOWLEDGMENTS

We thank L. Menéndez de la Prida, A. Fernandez-Ruiz, A. Navas-Olivé, R. Huszar, E. Barrio-Alonso, and members of our laboratory for helpful comments on the project.

Funding:

This work was supported by the European Molecular Biology Organization (EMBO) postdoctoral fellowship (EMBO ALTF 1161-2017) and Human Frontiers Science Program (HFSP) postdoctoral fellowship (LT0000717/2018) to M.V.; a Leon Levy Neuroscience Fellowship to I.Z.; and NIH MH107396, NS 090583, NSF PIRE grant (1545858), U19 NS107616, U19 NS104590, and NSF NeuroNex MINT grant 1707316.

Data and material availability:

E.Y. is inventor on patents applications US Patent 9,247,889 (2016) and US Patent 9,642,545 (2017) held by the University of Michigan that covers the neural probes with optical stimulation capability. All data needed to evaluate the conclusions are present in the paper and/or the supplementary materials and are publicly available in the Buzsaki Lab Databank: https://buzsakilab.com/wp/public-data/. Custom MATLAB scripts can be downloaded from https://github.com/buzsakilab/buzcode.

REFERENCES AND NOTES

1. Grienberger C, Milstein AD, Bittner KC, Romani S, Magee JC, Nat Neurosci. 20, 417–426 (2017). [PubMed: 28114296]
2. Petersen CCH, Neuron 95, 1266–1281 (2017). [PubMed: 28910617]
3. Long MA, Lee AK, Curr. Opin. Neurobiol 22, 34–44 (2012). [PubMed: 22054814]
4. Valero M, English DF, J. Neurosci. Methods 326,108397 (2019). [PubMed: 31400358]
5. Karnani MM, Agetsuma M, Yuste R, Curr. Opin. Neurobiol 26, 96–102 (2014). [PubMed: 24440415]
6. Csicsvari J, Hirase H, Czurkó A, Mamiya A, Buzsáki G, J. Neurosci 19, 274–287 (1999). [PubMed: 9870957]
7. Atallah BV, Scanziani M, Neuron 62, 566–577 (2009). [PubMed: 19477157]
8. Borg-Graham LJ, Monier C, Frégnac Y, Nature 393, 369–373 (1998). [PubMed: 9620800]
9. Mariño J et al., Nat. Neurosci 8, 194–201 (2005). [PubMed: 15665876]
10. Wehr M, Zador AM, Nature 426, 442–446 (2003). [PubMed: 14647382]
11. Bhatia A, Moza S, Bhalla US, eLife 8, e43415 (2019). [PubMed: 31021319]
12. Anderson JS, Carandini M, Ferster D, J. Neurophysiol 84, 909–926 (2000). [PubMed: 10938316]
13. Wilson RI, Nicoll RA, Nature 410, 588–592 (2001). [PubMed: 11279497]
14. Barron HC, Vogels TP, Behrens TE, Ramaswami M, Proc. Natl. Acad. Sci. U.S.A 114, 6666–6674 (2017). [PubMed: 28611219]
15. Wu F et al., Neuron 88, 1136–1148 (2015). [PubMed: 26627311]
16. Buzsáki G, Leung LW, Vanderwolf CH, Brain Res. 6, 139–171 (1983).
17. O'Keefe John., Nadel L, The Hippocampus as a Cognitive Map (Clarendon, 1978).
18. Mizuseki K, Diba K, Pastalkova E, Buzsáki G, Nat. Neurosci 14, 1174–1181 (2011). [PubMed: 21822270]
19. Wilson MA, McNaughton BL, Science 261, 1055–1058 (1993). [PubMed: 8351520]
20. Wilson MA, McNaughton BL, Science 265, 676–679 (1994). [PubMed: 8036517]
21. Lopes-dos-Santos V, Ribeiro S, Tort ABL, J. Neurosci. Methods 220, 149–166 (2013). [PubMed: 23639919]
22. Pfeiffer BE, Foster DJ, Nature 497, 74–79 (2013). [PubMed: 23594744]
23. Grosmark AD, Buzsáki G, Science 351, 1440–1443 (2016). [PubMed: 27013730]
24. Bittner KC et al., Nat. Neurosci 18, 1133–1142 (2015). [PubMed: 26167906]
25. Dragoi G, Harris KD, Buzsáki G, Neuron 39, 843–853 (2003). [PubMed: 12948450]
26. Lee D, Lin B-J, Lee AK, Science 337, 849–853 (2012). [PubMed: 22904011]
27. Samsonovich A, McNaughton BL, J. Neurosci 17, 5900–5920 (1997). [PubMed: 9221787]
28. Dragoi G, Tonegawa S, Nature 469, 397–401 (2011). [PubMed: 21179088]
29. McKenzie S et al., Neuron 109, 1040–1054.e7 (2021). [PubMed: 33539763]
30. O'Keefe J, Burgess N, Nature 381, 425–428 (1996). [PubMed: 8632799]
31. O'Keefe J, Krupic J, Physiol. Rev 101, 1427–1456 (2021). [PubMed: 33591856]
32. Cohen JD, Bolstad M, Lee AK, eLife 6, e23040 (2017). [PubMed: 28742496]
33. English DF et al., J. Neurosci 34, 16509–16517 (2014). [PubMed: 25471587]
34. Valero M et al., Nat. Neurosci 18, 1281–1290 (2015). [PubMed: 26214372]
35. Valero M et al., Neuron 94, 1234–1247.e7 (2017). [PubMed: 28641116]
36. Hulse BK, Lubenov EV, Siapas AG, Cell Rep. 18, 136–147 (2017). [PubMed: 28052244]
37. Buzsáki G, Hippocampus 25, 1073–1188 (2015). [PubMed: 26135716]
38. Joo HR, Frank LM, Nat. Rev. Neurosci 19, 744–757 (2018). [PubMed: 30356103]
39. Foster DJ, Annu. Rev. Neurosci 40, 581–602 (2017). [PubMed: 28772098]

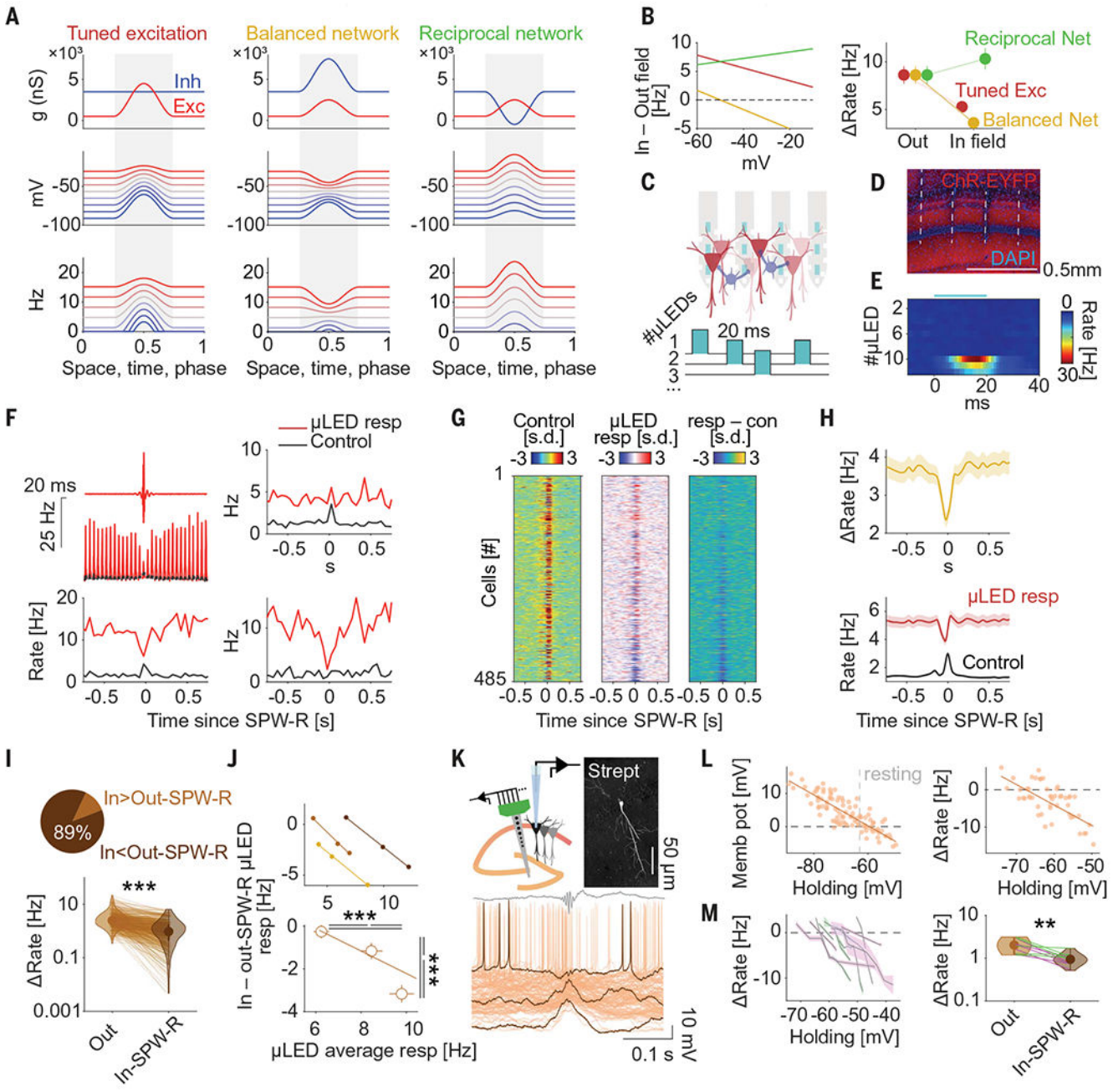

Fig. 1. Decreased single-neuron excitability during SPW-Rs.

(**A**) Different relationships of the excitatory and inhibitory conductances (top row) lead to specific membrane potential (middle row) and firing rate (bottom row). (**B**) Rate predictions as a function of the holding *V*m. (**C**) CA1 neurons in CamKIIα-Cre::Ai32 mice respond to 20-ms random pulses. (**D**) Probe shank locations. (**E**) Peristimulus time histogram (PSTH) from a pyramidal cell responding to three mLEDs on the same shank but not one to nine μLEDs on different shanks. (**F**) (Top left) Histograms showing responses to light pulses (red) and control rate (black dashed line) during SPW-Rs (30 bins of 50 ms). (Bottom) Response displayed for the same single neuron. (Right) Two other example cells.

(**G**) Z-scored control rate (left), optogenetic responses (center), and rate change (ΔRate = μLED responses – control; right) during SPW-Rs for all light-responding cells ranked by lightresponse amplitude. (**H**) Group control firing rate (black), light response rate (red) [mean ± confidence interval at 95%(CI95), bottom], and rate difference (gold; mean ± CI95). (**I**) Optogenetic responses decreased during SPW-Rs (ΔRate; $n = 485$ neurons; $P < 10^{-55}$,Wilcoxon paired signed-rank test) (**J**) (Top) Difference between in-SPW-R versus outside SPW-R firing rates as a function of three light intensities in three neurons. (Bottom) Population average (mean ± CI95 $\rho = -0.55$, $P < 10^{-57}$; $P < 10^{-9}$ for all comparisons, Friedman test). (**K**) Pyramidal neuron filled with biocytin from a head-fixed waking mouse experiment. (Bottom) Responses of the filled neuron at different V_m (three traces are highlighted in black) during SPW-Rs (top gray line, average ripple). (**L**) Relationship between the holding V_m and V_m change (left) and firing-rate change (right) for all SPW-R in (K). (**M**) Group results for five cells from five anesthetized rats (green) and five cells from four head-fixed mice (pink). (Right) Decreased gain during SPW-Rs ($P = 0.002$; Wilcoxon paired signed-rank test). $^{**}P < 0.01$ and $^{***}P < 0.001$.

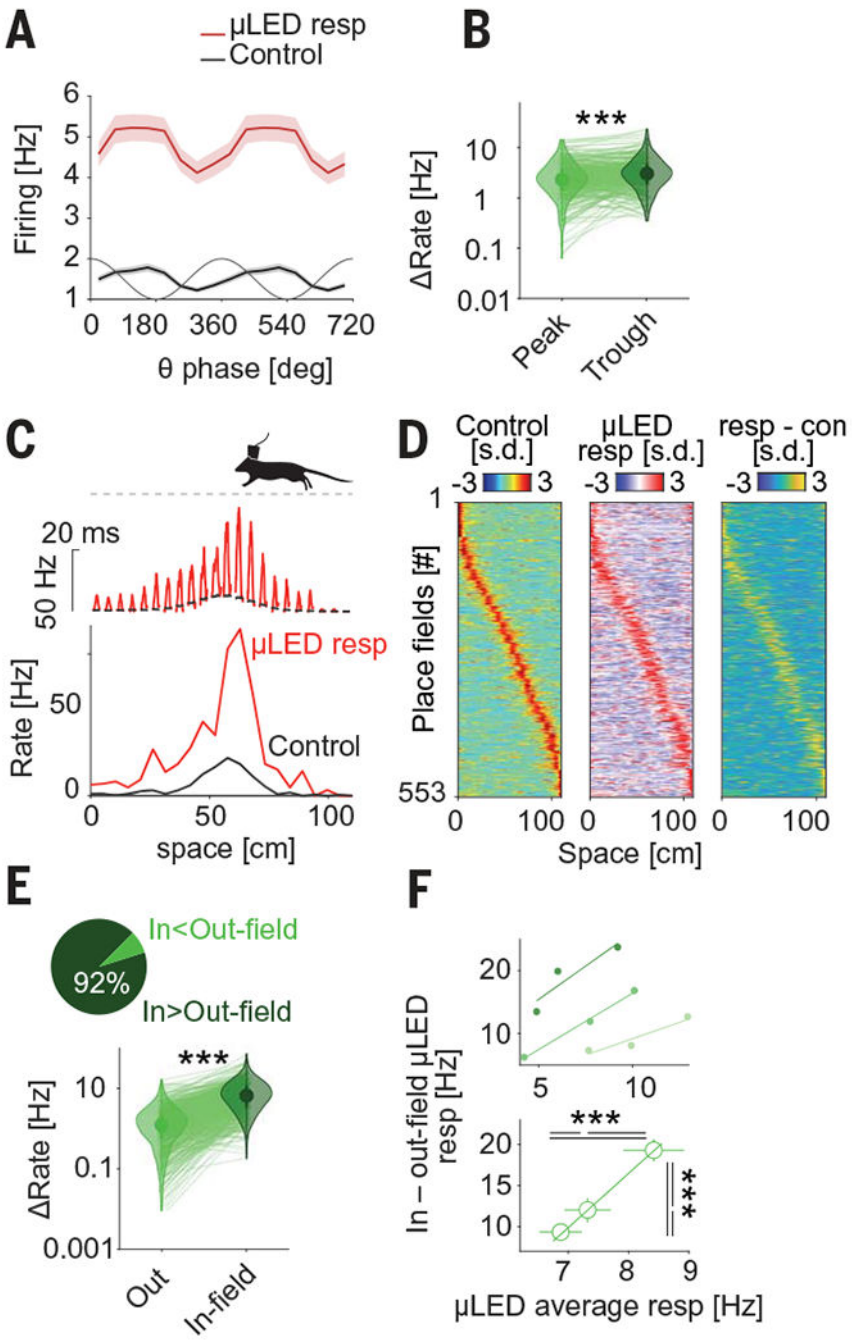

Fig. 2. Increased excitability during theta oscillations and within place fields.

(**A**) Thin line, theta phase. Red and black lines, phase histograms of spikes during optostimulation and control pulses, respectively (mean ± CI95). (**B**) Rate gain at the trough of the theta cycle ($P < 10^{-6}$, Wilcoxon test). (**C**) (Top) Light-induced spike histograms (red line) and control rate (black line). (Bottom) for the same single neuron. (**D**) Control, light responses and difference (resp–con) for all light-responsive neurons, ranked by the control rate peak position. (**E**) Responses were larger inside than outside the place field (n = 553 place fields; $P < 10^{-115}$; Wilcoxon test). (**F**) (Top) Difference between in-field and

out-of-field firing rates (gain), as a function of three light intensities in three neurons (top) and group average (bottom; $\rho = 0.24$, $P < 10^{-6}$; $P < 10^{-8}$, Friedman test). ***$P < 0.001$.

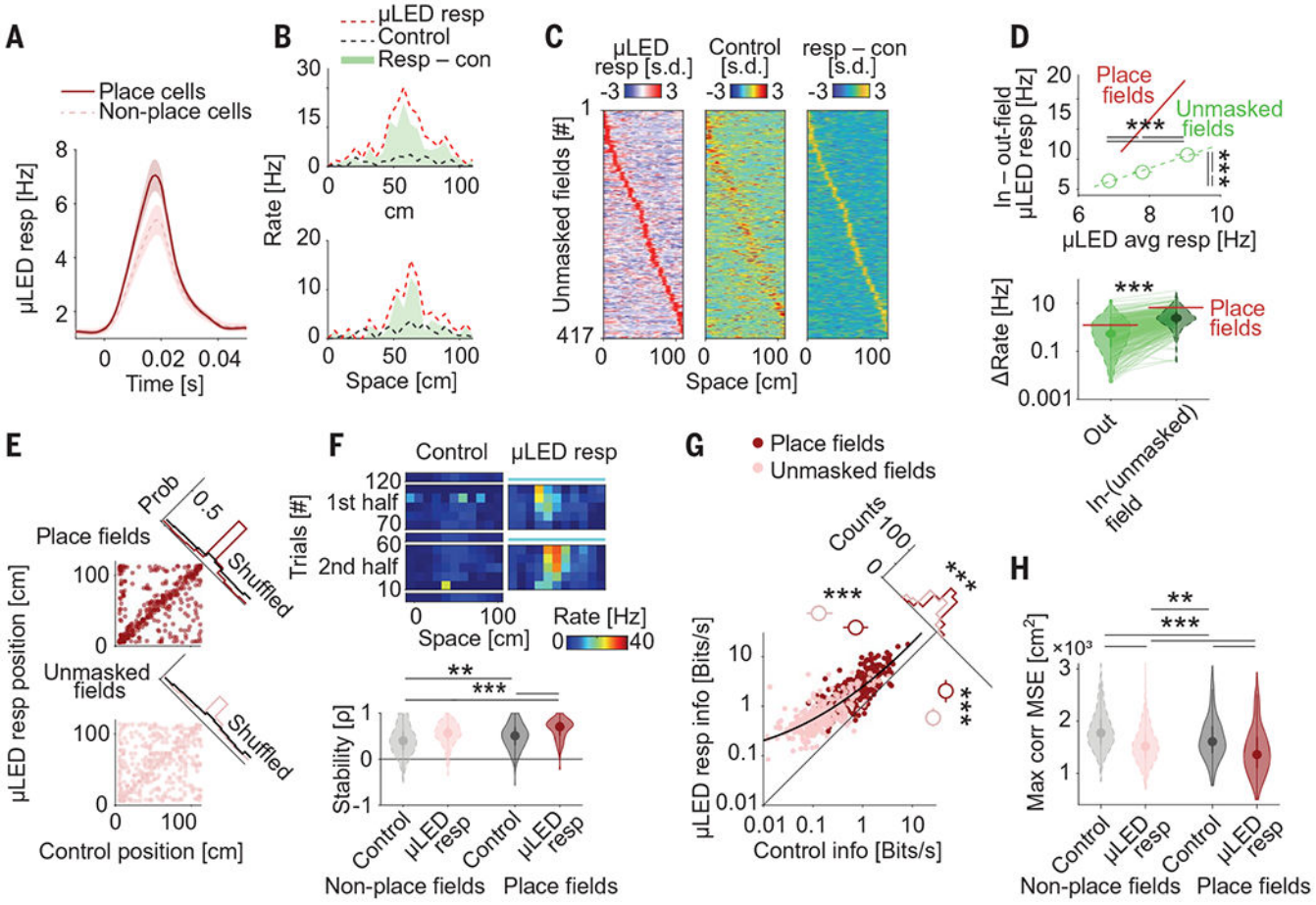

Fig. 3. Unmasking subthreshold place fields.

(**A**) Evoked responses in home cage sessions in place cells and non–place cells [$P < 10^{-4}$, Kruskal–Wallis (KW) test]. (**B**) Light responses (red) and control (black) spikes for two example non–place neurons. (**C**) Light-induced place fields, control spike rate, and rate gain during light stimulation for all light-responding non–place cells ranked by the light responses. (**D**) Difference between in-field and out-of-field firing rates at three light intensities ($P < 10^{-56}$, Wilcoxon paired test; $\rho = 0.38$, $P < 10^{-5}$ for all comparisons, Friedman test). For comparison, the slope from place cells (Fig. 2F) is superimposed. (**E**) Correlation between peak location in control epochs and light responses for place fields of place cells (top, $P < 10^{-40}$, χ^2 test against 500 shuffles) and unmasked place fields of non–place cells (bottom; $P < 10^{-10}$, χ^2 test). (**F**) Spike activity for an example non–place cell during baseline (no stimulation) runs (1 to 10, 61 to 70, 121 to 130) and stimulation runs. Spike activity during light stimulation (20-ms pulses; right panel) and between stimulation (control) epochs (left panel). Correlation between first and second halves (trials 11 to 60 and 71 to 120) of the session was used to compute place field stability. (Bottom) Place fields during light stimulation were more stable for both true place fields and unmasked place fields [$P < 10^{-9}$ and $P < 10^{-19}$, respectively; two-ways analysis of variance (ANOVA)] than during control epochs. (**G**) Correlation of spatial information (Bits/spike) between control and light-stimulated epochs ($P < 10^{-62}$ and $P < 10^{-58}$, respectively; KW test). Black line

shows an exponential fit. Light-boosted effect was stronger for unmasked place fields of non–place cells than for place cell place fields ($P < 10^{-15}$; KW test). (**H**) Spatial decoding accuracy of the mouse's position on the track increased during light-stimulation epochs of both non–place cells and place cells ($P < 10^{-8}$ and $P < 10^{-27}$ for control and light epochs, respectively; two-way ANOVA). Note lower mean squared error (MSE) during light stimulation of non–place cells compared to control spiking of place cells ($P = 0.001$, Tukey test). $^{**}P < 0.01$ and $^{***}P < 0.001$.

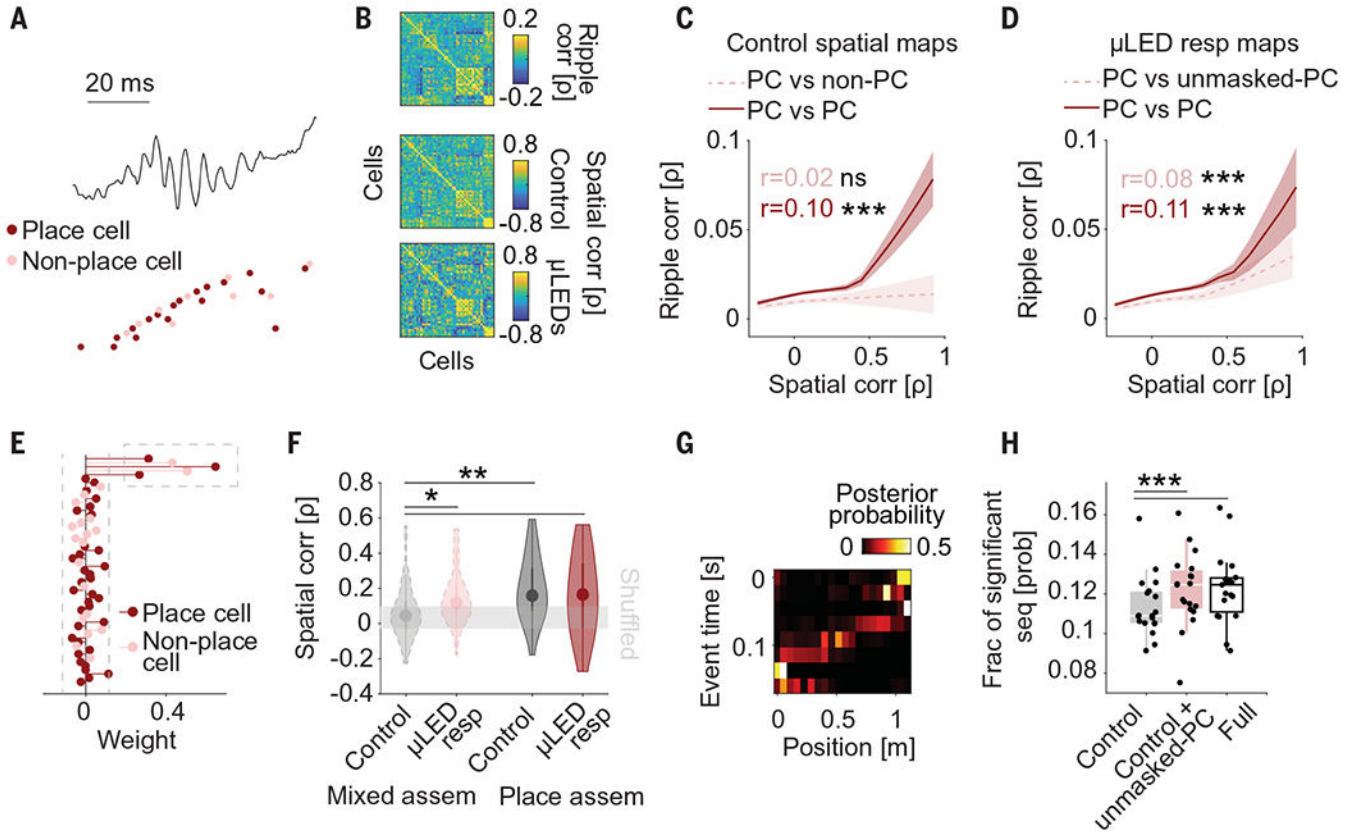

Fig. 4. Uncovering spatial overlap of preexisting cell ensembles.

(**A**) Neural sequence of place cells and non–place cells during a SPW-R. (**B**) Similarity matrices show cofiring of 47 pyramidal neurons in an example session during SPW-R in the home cage and spatial correlations of the same pairs (Spearman's ρ) during control and light-stimulation epochs on the track. (**C**) SPW-R cofiring was positively correlated with spatial overlap in place cell pairs ($P < 10^{-27}$, Spearman correlation) but not in pairs with place and non–place cell (non-PC) partners ($P = 0.11$). (**D**) Same as (C), but for light-induced responses ($P < 10^{-5}$, Spearman correlation; $P < 10^{-29}$ for place cell pairs; $P = 0.002$ between control and light stimulation after correcting by the spatial cofiring; repeated-measures ANOVA). (**E**) Cell assemblies (21) in home cage recordings. Relative weights of neuron in an example assembly. Neurons with > 2 SDs (dashed gray line) of the weight distribution were classified as members of the assembly. (**F**) Spatial overlap on the track (ρ) was higher among assemblies consisting of only–place cells than for assemblies of mixed place cells and non–place cells ($P = 0.006$, $P = 0.31$, and $P = 0.02$ for assemblies, light stimulation, and their interaction, respectively; two-way ANOVA). (**G**) Forward replay sequence during home cage recording. Bayesian decoding (22). (**H**) The fraction of SPW-R events with significant trajectories (against 500 shuffles) increased ($P < 10^{-4}$, Friedman test) when unmasked place fields of non–place cells ($P < 10^{-4}$, Tukey test) and when spikes from both stimulated place fields and unmasked place fields ($P < 10^{-3}$) were included for the construction of the place field sequence template. *$P < 0.05$, **$P < 0.01$ and ***$P < 0.001$.